Exchange of warming deep waters across Fram Strait

Wilken-Jon von Appen [a,*], Ursula Schauer [a], Raquel Somavilla [a,1], Eduard Bauerfeind [a], Agnieszka Beszczynska-Möller [b]

[a] Alfred Wegener Institute, Helmholtz Centre for Polar and Marine Research, Am Handelshafen 12, 27570 Bremerhaven, Germany
[b] Institute of Oceanology PAS, Sopot, Poland

A B S T R A C T

Current meters measured temperature and velocity on 12 moorings from 1997 to 2014 in the deep Fram Strait between Svalbard and Greenland at the only deep passage from the Nordic Seas to the Arctic Ocean. The sill depth in Fram Strait is 2545 m. The observed temperatures vary between the colder Greenland Sea Deep Water and the warmer Eurasian Basin Deep Water. Both end members show a linear warming trend of 0.11 ± 0.02 °C/decade (GSDW) and 0.05 ± 0.01 °C/decade (EBDW) in agreement with the deep water warming observed in the basins to the north and south. At the current warming rates, GSDW and EBDW will reach the same temperature of -0.71 °C in 2020. The deep water on the approximately 40 km wide plateau near the sill in Fram Strait is a mixture of the two end members with both contributing similar amounts. This water mass is continuously formed by mixing in Fram Strait and subsequently exported out of Fram Strait. Individual measurements are approximately normally distributed around the average of the two end members. Meridionally, the mixing is confined to the plateau region. Measurements less than 20 km to the north and south have properties much closer to the properties in the respective basins (Eurasian Basin and Greenland Sea) than to the mixed water on the plateau. The temperature distribution around Fram Strait indicates that the mean flow cannot be responsible for the deep water exchange across the sill. Rather, a coherence analysis shows that energetic mesoscale flows with periods of approximately 1–2 weeks advect the deep water masses across Fram Strait. These flows appear to be barotropically forced by upper ocean mesoscale variability. We conclude that these mesoscale flows make Fram Strait a hot spot of deep water mixing in the Arctic Mediterranean. The fate of the mixed water is not clear, but after the 1990s, it does not reflect the properties of Norwegian Sea Deep Water. We propose that it currently mostly fills the deep Greenland Sea.

1. Introduction

The deep ocean circulation of the Nordic Seas and the Arctic Ocean is isolated from the World Ocean below 800 m (sill depth of the Faroe Bank Channel). The region between the west coast of Svalbard and the east coast of Greenland is known as Fram Strait (Fig. 1). The eastern side of Fram Strait is a wide flat area of about 2500 m depth. Here we consider this plateau in Fram Strait to be the area away from the continental slopes roughly encompassed by the 2300 m and 2700 m isobaths. The sill with a depth of 2545 m according to the International Bathymetric Chart of the Arctic Ocean (IBCAO, Jakobsson et al., 2012) is located just east of 0°E and south of 79°N. The Greenland Sea is located to the south of Fram Strait while the Eurasian Basin of the Arctic Ocean is to the

north and both are deep (> 3000 m) basins. The waters at depths of more than 2000 m in these basins are known as Greenland Sea Deep Water (GSDW) and Eurasian Basin Deep Water (EBDW) respectively (Aagaard et al., 1985; Swift and Koltermann, 1988; Somavilla et al., 2013). The Norwegian Sea is further to the south east of Fram Strait and contains Norwegian Sea Deep Water (NSDW) at depths >2000 m. Swift and Koltermann (1988) found water in the Norwegian Sea with similar temperature-salinity characteristics to what they had measured in Fram Strait. Based on this, they hypothesized that mixing in the deep Fram Strait could be the origin of Norwegian Sea Deep Water.

Changes in the frequency and water mass percentage of different water masses flowing through the deep Fram Strait have been studied from repeated east–west CTD sections along 78°50′N (Langehaug and Falck, 2012). This analysis was based on constant temperature–salinity end member definitions derived from observational studies in the 1980s (Swift and Koltermann, 1988). Specifically, no changes in the end member properties were considered in the analysis of Langehaug and Falck (2012). As a result of
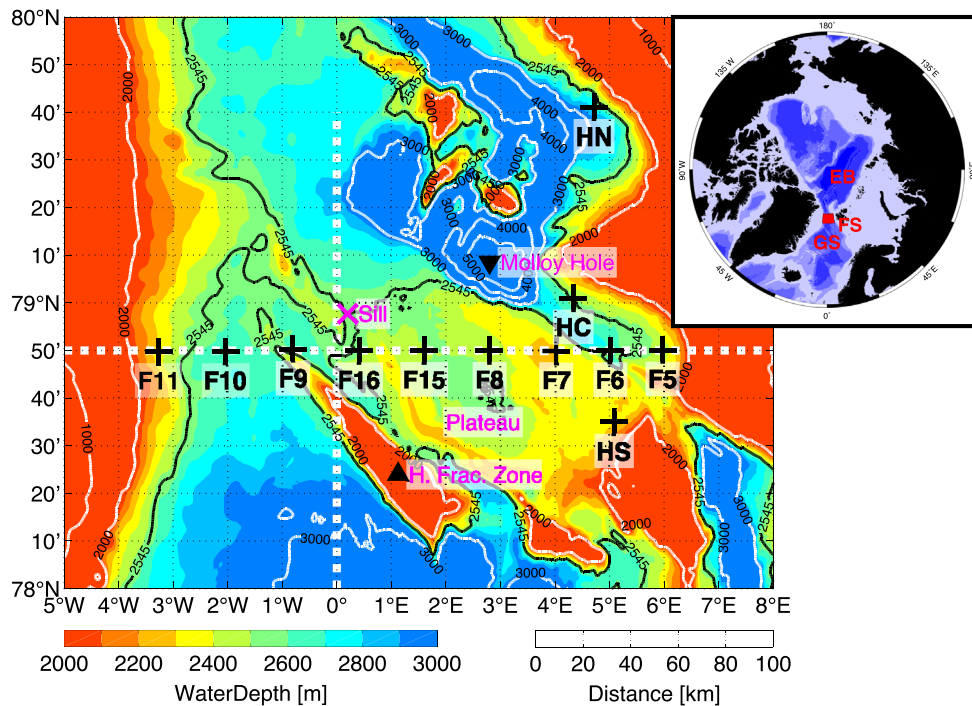
Fig. 1. Map of the bathymetry around the Fram Strait sill from IBCAO version 3.0 (Jakobsson et al., 2012). Only water depths from 2000 m to 3000 m are shown in color to highlight the bathymetric features relevant for the bottom water. Based on this topographic data set, the sill is 2545 m deep and located just east of 0°E and south of 79°N; its isobath is also drawn as a thick black line. The Høvgaard Fracture Zone (1165 m depth) and the Molloy Hole (5573 m depth) are the shallowest and deepest points in the deep Fram Strait, respectively. A distance scale bar is given in the bottom right. The median locations of the deep moorings considered in this study are marked by black crosses: F5–11 and F15/16 along 78°50′N and the three Hausgarten moorings (HS, HC, HN) in the eastern Fram Strait. The extents of the zonal (along 78°50′N) and the meridional (along 0°E) CTD sections are marked by white dashed lines. The inset in the top right corner shows the whole Arctic. The extent of the main map is shown as a red polygon in relation to the Fram Strait ("FS") as well as the Greenland Sea ("GS") to the south and the Eurasian Basin ("EB") to the north. (For interpretation of the references to color in this figure legend, the reader is referred to the web version of this article.)

this the analysis concludes that GSDW completely disappeared from Fram Strait throughout the 2000s (Langehaug and Falck, 2012). However, repeated CTD stations in the Greenland Sea show that GSDW has been warming at a (for deep waters rapid) pace of ≈ 0.14 °C/decade (Somavilla et al., 2013) from values of -1 °C in the 1990s to > -0.8 °C in the late 2000s for $\theta_{2.5}$ (potential temperature relative to 2500 dbar) around 2500 m depth which is close to the sill depth of Fram Strait. Following the halt of deep convection in the Greenland Sea in the early 1990s (Schlosser et al., 1991; Rhein, 1991; Meincke et al., 1992), the warming of the deep Greenland Sea is explained by the continuous inflow of the warmer EBDW to the Greenland Sea across Fram Strait (Aagaard et al., 1991; Somavilla et al., 2013). That is, the Greenland Sea has a heat source, but no longer a heat sink and therefore is in a non-stationary state and warms.

The exchange of deep water across Fram Strait required to account for the warming (and increase in salinity) of the Greenland Sea was estimated as 0.4 Sv (1 Sv $= 10^6$ m^3/s) (Somavilla et al., 2013). However, there should not be an associated net volume flux across Fram Strait (at least not unless there are huge and unrealistic vertical displacements of isopycnals below ≈ 2000 m in the Arctic Ocean to the north and the Nordic Seas to the south) which implies a balancing northward transport of 0.4 Sv. The exchange could also be achieved solely by eddy diffusion across Fram Strait and no steady mean currents are required in order to explain the warming of the deep Greenland Sea. Tracer release experiments in a coarse resolution numerical model (Marsh et al., 2008) showed that the flow across Fram Strait was inhibited below 2100 m in the 1990s, but there was an indication of exchange and the propagation of Greenland Sea Deep Water into the Eurasian Basin in the 2010s (Y. Aksenov personal communication). Gridded velocities from a multi-year mooring array across Fram Strait

imply a mean meridional flow in the deep Fram Strait with flow to the north in the east and to the south in the west (Beszczynska-Möller et al., 2012). However, that depiction also corresponds to a mean net southward volume transport of 1.4 Sv below 1500 m, contrary to the expectation of zero mean net meridional transport. This is due to the sparse horizontal coverage of the moorings in Fram Strait. The Rossby radius of about 8 km in Fram Strait (Zhao et al., 2015) and bottom topographic features such as submarine valleys are not sufficiently resolved. In the upper water column of the eastern Fram Strait, the West Spitsbergen Current (WSC) transports warm Atlantic origin water northwards and the boundary current is barotropically unstable (Teigen et al., 2010) thereby generating eddies in the Fram Strait with a mostly barotropic structure. The resulting barotropic eddy field was described both from in situ and remote sensing observations (e.g. Johannessen et al., 1987; Manley et al., 1987). This Atlantic Water inflow to the Arctic Ocean has been observed to have warmed by 0.6 °C/decade above 1000 m throughout the late 1990s and 2000s (Beszczynska-Möller et al., 2012). We note, however, that this is a distinct process unrelated to the evolution of the deep waters in Fram Strait as discussed in the present study.

Straits and sills separating oceanic basins throughout the World Ocean have received considerable attention because they influence the interface height of isopycnals in the basins. If the horizontal density gradient across the sill is large, energetic flows result downstream of the sill that mix and entrain waters thereby transforming water masses. Examples are Denmark Strait (Nikolopoulos et al., 2003), the Strait of Gibraltar (Price and O'Neil Baringer, 1994), and the Samoan Passage in the deep Pacific (Alford et al., 2013). What are then the gradients across the deep Fram Strait and the associated flow structure? How is the exchange of the deep waters across Fram Strait achieved and where does the

associated mixing take place? To answer these questions, we use the data described in Section 2. Section 3 then presents the temperature trends observed in the deep Fram Strait. The meridional extent of the mixing region is investigated in Section 4. The bottom velocity structure and the forcing mechanisms of the velocities are explained in Section 5. Finally, we close with a summary and discussion of the fate of the mixed water in Section 6.

2. Data and methods

2.1. Moorings

From 1997 onwards, a mooring array as well as three individual moorings have been maintained in Fram Strait (Table 1) by the physical oceanography group of the Alfred Wegener Institute (F5–F10 and F15/F16; Beszczynska-Möller et al., 2012), the Norwegian Polar Institute (F11; de Steur et al., 2009), and the Hausgarten Deep Sea Observatory group of the Alfred Wegener Institute (HS="Hausgarten South", HC="Hausgarten Central", HN="Hausgarten North"; Bauerfeind et al., 2009). Here we focus on the records from the current meters closest to the bottom. These were Aanderaa RCMs (Rotor Current Meter: RCM7 and RCM8; Doppler Current Meter: RCM11) often measuring pressure and always measuring speed, direction, and temperature; salinity was not measured by the RCMs. Their temporal resolution ranged from 20 min to 2 h depending on the instruments and deployment durations. Pre-deployment instrument calibration at the manufacturers was carried out as a standard procedure and achieved an accuracy of $\pm 0.05\,°C$ for temperature, of max(± 0.01 m/s, $\pm 4\%$) for RCM7/8 and of max(± 0.0015 m/s, $\pm 1\%$) for RCM11 for speed, and of $\pm (5\text{--}7.5)°$ for direction. We note that the values for temperature are similar to the range of the signals as observed and described in this study. Post-cruise instrument calibration at the manufacturers was generally not performed. CTD profiles (see Section 2.2 below) were taken in the vicinity of the mooring locations during the mooring deployment and recovery cruises. The moored temperature timeseries were checked for offsets and drifts by comparison to the CTD casts. If a timeseries exhibited an offset or drift, it was removed. All temperature timeseries discussed here are derived from multiple consecutive deployments of different instruments in the same location. If there had been instrument drifts on the order of the observed temperature trends, then records from consecutive instruments would not have fit together. The fact that this was not observed increases the reliability of the measurements as they are not just derived from a single moored

instrument with its accuracy/precision limitations. From 2010 onwards, mooring HC also contained a near-bottom Seabird SBE37 microcat. This provides the only mooring based salinity timeseries in the deep Fram Strait. We also use velocity data from RCMs located in the upper water column ≈ 75 m below the surface on mooring F10.

Except for the Hausgarten moorings, the moorings are deployed along a zonal section along 78°50′N (Fig. 1). However, up until 2002, the western-most part of the array (F9–F11) was located at 79°N and at 78°50′N thereafter. For the temperature timeseries analysis, we consider these moorings only after their relocation. All of the moorings have been deployed until at least 2014, but some have not been recovered or processed yet and we therefore focus on the available records here as summarized in Table 1. The data from these moorings are available in the Pangea database (von Appen et al., 2015).

2.2. CTD measurements

A zonal section of Conductivity–Temperature–Depth (CTD) profiles in Fram Strait along 78°50′N (Fig. 1) has been occupied every summer since 1997 as part of the mooring service cruises. Seabird 911+ systems were used and standard pre-cruise plus bottle salinity calibration was applied to all of the profiles. In 1997, 1998, 1999, 2001, and 2002, a meridional section along 0°E (Fig. 1) was also occupied. The data from all of these CTD sections are available in the Pangea database (von Appen et al., 2015).
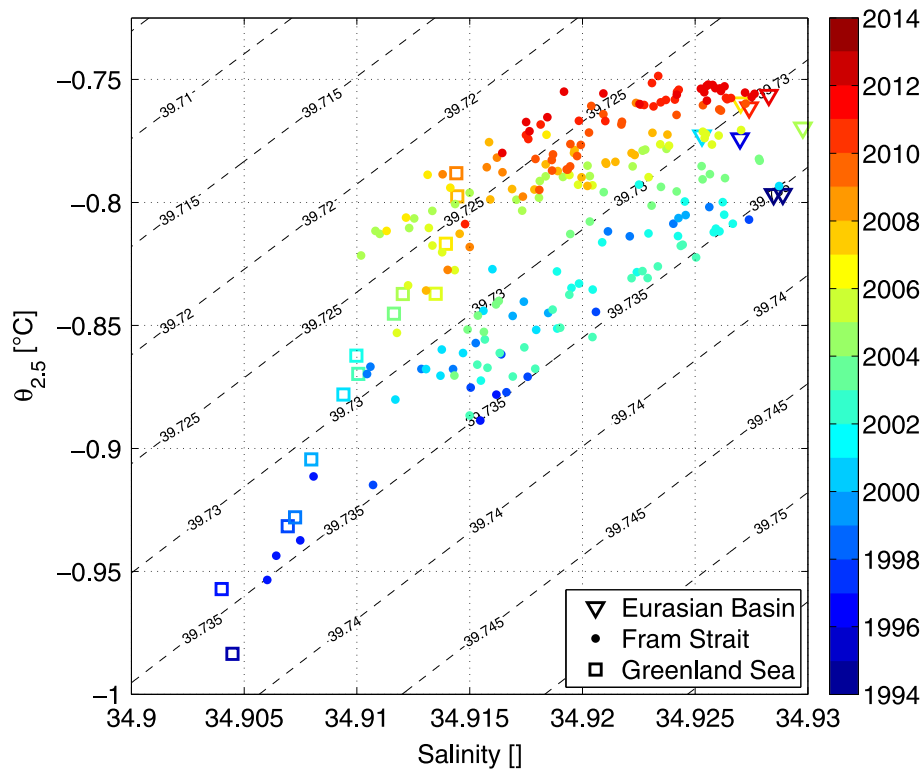
Deep CTD casts in the Greenland Sea and the Eurasian Basin as compiled and presented by Somavilla et al. (2013) are also used in this study. The averages of the CTD casts in each of the years are computed for the two basins (central Greenland Sea: 74°N–76°N, 6°W–0°E; Eurasian Basin: 85°N–88°N, 30°E–140°E) from the data obtained from the ICES (http://www.ocean.ices.dk) and Pangea (http://www.pangea.de) databases. Additionally, we use CTD profiles from the World Ocean Database (http://www.nodc.noaa.gov/OC5/WOD/pr_wod.html) in the Norwegian Sea (confined by the Mohns Ridge, the Jan Mayen Ridge, the Greenland-Scotland Ridge, and the continental slope of Norway).

2.3. Bathymetry

The bathymetry depicted in this study is from the International Bathymetric Chart of the Arctic Ocean (IBCAO) in its version 3.0 (Jakobsson et al., 2012). In the region discussed in this study, the IBCAO grid at depths greater than 2000 m is entirely based on multi-beam data (compare the source identification grids provided by the project at http://www.ibcao.org). This is due to the large number of ship-based expeditions to this region over the past two decades.

2.4. Calculation of potential temperature

Throughout this study we consider the potential temperature (and likewise potential density anomaly) with respect to a reference pressure of 2500 dbar: $\theta_{2.5}$ and $\sigma_{2.5}$. The sill depth of Fram Strait is close to this depth and most of the deep moored instruments are close to 2500 m making $\theta_{2.5}$ an adequate choice to discuss deep exchange flows. Salinity is required to calculate potential temperature, but the moorings did not contain salinity measurements. However, the range of salinities in the deep water (34.905–34.93, Fig. 2) is very small in terms of its effect on potential temperature. Therefore, for the records without salinity, we use a constant salinity of 34.92 for the calculation of potential temperature.

Table 1
Deployment details of the 12 moorings considered in this study. Over the years, the mooring locations slightly varied as indicated by the ranges. The instruments were deployed between 10 m and 100 m above the bottom.

| Mooring name	Longitude range	Latitude range	Instrument depth range (m)	Duration
F5	5°51′E – 6°28′E	78°49′N – 78°50′N	1993–2500	1997–2012
F6	5°00′E – 5°03′E	78°50′N – 78°50′N	2667–2698	1997–2012
F7	4°00′E – 4°05′E	78°49′N – 78°51′N	2302–2346	1997–2012
F8	2°34′E – 2°48′E	78°50′N – 78°50′N	2463–2505	1997–2014
F15	1°36′E – 1°37′E	78°50′N – 78°50′N	2504–2529	2002–2014
F16	0°23′E – 0°32′E	78°50′N – 78°50′N	2550–2567	2002–2012
F9	0°49′W – 0°16′E	78°50′N – 79°00′N	2489–2656	1997–2012
F10	2°07′W – 2°00′W	78°49′N – 79°01′N	2589–2702	1997–2012
F11	3°38′W – 3°01′W	78°48′N – 79°01′N	2126–2503	1998–2012
HS	5°02′E – 5°06′E	78°35′N – 78°36′N	2225–2334	2004–2011
HC	4°20′E – 4°21′E	79°00′N – 79°02′N	2521–2584	2001–2014
HN	4°04′E – 5°10′E	79°36′N – 79°44′N	2537–2774	2004–2012

Fig. 2. Depth mean (2500–2525 m) potential temperature and salinity. The individual CTD profiles in Fram Strait (within 78°49′N–79°01′N, 2°30′W–5°30′E) are shown as dots colored by the year of the measurement. The means over the basins of the depth averaged (2500–2525 m) $\theta_{2.5}S$ are shown as empty colored squares (Greenland Sea) and triangles (Eurasian Basin). Potential density $\sigma_{2.5}$ [kg/m^3] is shown in contours. (For interpretation of the references to color in this figure legend, the reader is referred to the web version of this article.)

## 3. Trends of deep temperatures in Fram Strait

The waters in the Greenland Sea and the Eurasian Basin changed in temperature and salinity from the mid 1990s to the mid 2010s with GSDW warming and becoming saltier since the halt of deep convection in the Greenland Sea (Somavilla et al., 2013). We use the depth average CTD properties between 2500 m and 2525 m, slightly above the sill level of 2545 m in Fram Strait and close to the depth of the mooring records, but we note that the results discussed here do not depend on the exact depth of averaging above the sill level. The depth averages (2500–2525 m) of the CTD profiles were taken here to reduce the single measurement noise compared to picking out a single depth (e.g. exactly 2500 m). The evolution of the potential temperature and salinity averaged over the whole Greenland Sea (as defined in section 2.2) from 1994 onwards (Fig. 2) shows the clear warming (from ≈ − 1 °C to > − 0.8 °C) and salinity increase (from >34.905 to ≈ 34.915). The Eurasian Basin (as defined in Section 2.2) is visited only infrequently by research ice-breakers resulting in a smaller number of years with basin average profiles. The available data (Fig. 2) points to a small warming of ≈ 0.05 °C over approximately 20 years while a salinity trend is not detectable within the noise level. Comparison of individual profiles in the Eurasian Basin (not shown) confirms that the warming is occurring without a salinity change. The warming in the Eurasian Basin reduced the in situ density by about 0.005 kg/m^3. In the Greenland Sea, the warming would have reduced its density at sill level by ≈ 0.02 kg/m^3. However, due to the concurrent increase in salinity, the actual density decrease was only a bit more than 0.01 kg/m^3. While in the early 1990s, the density at sill level in the Greenland Sea was higher than in the Eurasian Basin, it was lower in the Eurasian Basin in the 2010s. This might have impacts on the exchange flow across the Fram Strait sill if the exchange flow was density driven.

The 2500–2525 m depth averages of the individual CTD casts in the deep Fram Strait (Fig. 2) clearly show that they fall in between the temperature and salinity values observed in the central Greenland Sea and Eurasian Basin. For each of the years, the measurements are scattered roughly along the in situ density lines with the trend towards lighter water in the later records visible. Therefore, we consider the water masses observed in the central basins (GSDW=Greenland Sea Deep Water and EBDW=Eurasian Basin Deep Water) as end members for the observations in Fram Strait which at each point in time can be explained as a linear combination of the two end members. The observations in Fram Strait (Fig. 2) also show that the water in the deep Fram Strait is distributed relatively randomly between the two end members.

The warming of the end members is also reflected in the 17 years (1997–2014) potential temperature records from the seven deep moorings (F6–10, F15/16) along the zonal section across Fram Strait (Fig. 3). There is considerable year-to-year variation at the same location associated with yearly summer turn-around of the instruments. The timeseries vary between a warm and a cold end member, both of which have been warming over time. As shown above, these end members are GSDW (cold) and EBDW (warm). At each mooring we define the envelopes of the temperature curves as the 2nd and the 98th percentile of the temperature observations in 6 months long bins. A linear least squares trend was then fitted to these 6 monthly temperature upper/lower estimates. This procedure is adopted to deal with the fact that the temperature records are close to the accuracy and precision of the instruments. The use of the 2nd and the 98th percentile accounts for the precision limitation, i.e. it is expected that some of the measured values are lower/higher than the real temperatures. The 6 months long bins account for the changing accuracies of the different instruments (typical single instrument deployment durations of 1 or 2 years), i.e. some instruments are expected to be closer to the real
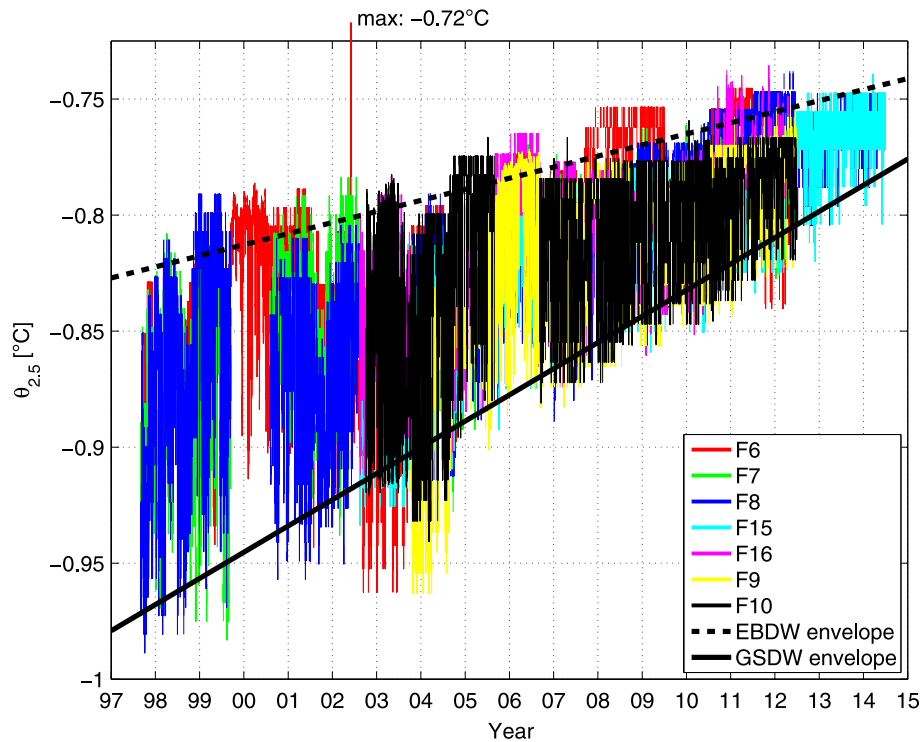
Fig. 3. Potential temperature [°C] relative to 2500 dbar timeseries from 1997 to 2014 of the deep moorings F6–10 and F15/16 along the main zonal section across Fram Strait. The timeseries are unfiltered data at their raw 20 min–2 h temporal resolution. The fitted envelopes for the GSDW and the EBDW end members are shown in black (see text for how they were constructed).
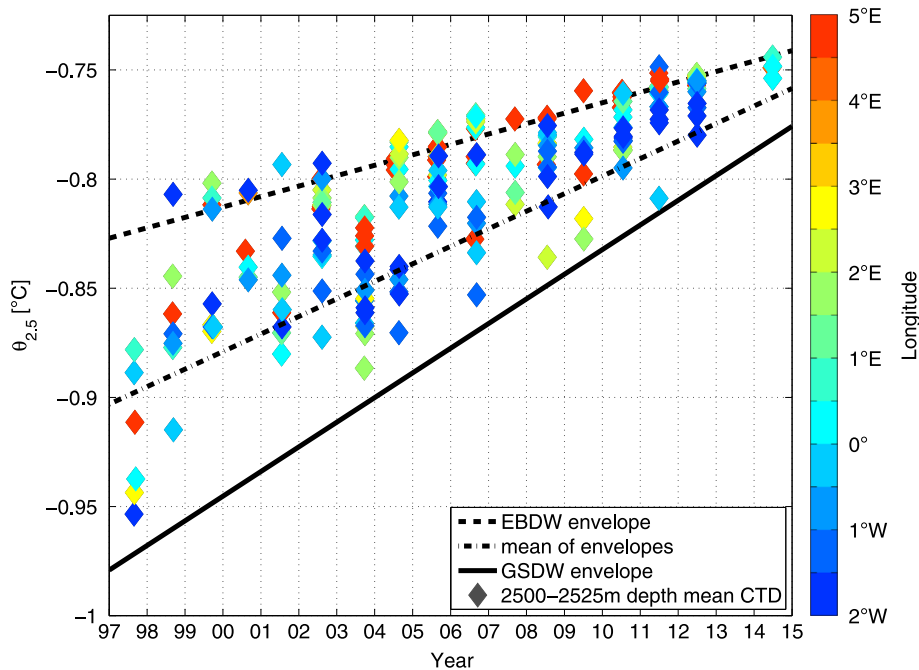
Fig. 4. Potential temperature measured by summer CTD casts along the main zonal section compared to the fitted GSDW and EBDW envelopes. The depth means (2500–2525 m) of each of the CTD profiles are shown as diamonds colored by their zonal location in the deep Fram Strait. The envelopes are identical to Fig. 3, and the mean of the envelopes used for the definition of the normalized temperature (see Eq. (1)) is also shown. (For interpretation of the references to color in this figure legend, the reader is referred to the web version of this article.)

value while others might be further off.

The linear trend of the potential temperature of the GSDW end member starts at -0.98 ± 0.02 °C (mean plus/minus standard deviation of the seven estimates from the individual moorings) in 1997 (January 1) and finishes at -0.78 ± 0.01 °C in 2015 (January 1) while the EBDW end member starts at -0.83 ± 0.01 °C in 1997

and finishes at -0.75 ± 0.01 °C in 2015. We note that the records from the different moorings are so close to each other (in particular there are also no systematic east–west differences) that slight differences in the definition do not have a substantial impact on the estimates of the trends. The average envelopes as shown in Figs. 3 and 4 are then defined as straight lines between the mean

starting (1997) and ending (2015) potential temperatures. From this we infer potential temperature trends of 0.11 ± 0.02 °C per decade for GSDW and 0.05 ± 0.01 °C per decade for EBDW. This establishes that GSDW is warming approximately twice as fast as EBDW. At the current rates, these two water masses would have the same potential temperature of −0.715 °C in early 2020. Presumably their mixing mechanism would therefore change qualitatively in or before 2020 and the different water masses would no longer be detectable from temperature alone. Based on the available records, a simple linear trend seems sufficient for an appropriate description of the available temperature observations, i.e. higher order polynomials are not required.

The potential temperatures at 2500–2525 m from the zonal summer CTD sections along 78°50′N (Fig. 4) show that most of the observations fall in between the envelopes, with a small number of observations above the EBDW envelope. There is no systematic zonal gradient across the deep Fram Strait (compare the colors in Fig. 4) with e.g. water on one side always being warmer than on the other side. It becomes clear that as a ship surveys the region at one point in time, it can pick out any of the situations between the end members. This complicates the interpretation of CTD sections for long term trends (e.g. Langehaug and Falck, 2012) as the long term trend is mixed with the variability on shorter time scales which will be described in detail below.

The potential temperature records from the Hausgarten moorings (Fig. 5) to the north and south of the main zonal section display some qualitative differences from the records at the moorings on the Fram Strait plateau (Fig. 3). Again, they roughly fall between the envelopes, but they do not reach the end members as frequently as on the plateau. From 2010 to 2014, HC was also equipped with a microcat achieving a much better temperature resolution than the current meters.

This allows the timeseries (Fig. 6) to be described as EBDW most of the time with intermittent events of colder water containing some percentage of GSDW lasting from a few hours to several days. There are two outliers compared to the temperature records between the envelopes. At HC, higher temperatures up to $\theta_{2.5} = -0.64$ °C were observed between April 25, 2002 and August 2, 2002 (Fig. 5) and during this time, there are also 17 individual recordings ($\Delta t = 2$ h during that deployment) clearly exceeding the envelopes (up to $\theta_{2.5} = -0.72$ °C) at F6 (Fig. 3). Then on July 13, 2013 and July 14, 2013, another 11 individual recordings ($\Delta t = 1$ h during that deployment) up to $\theta_{2.5} = -0.64$ °C were observed at HC. This temperature increase of 0.1 °C compared to the EBDW envelope was associated with a salinity increase of 0.01 meaning that it was not associated with a strong density anomaly. These temperature outliers are due to the propagation of a dense high salinity shelf plume through the measurement location. It originated in Storfjorden at the southern tip of Svalbard and entrained warm Atlantic layer water resulting in the higher temperatures. The plume passed the main zonal array higher up on the continental slope of Svalbard mainly in the vicinity of mooring F4, east of F5, as is discussed in detail in Akimova et al. (2011).

4. Meridional extent of mixed waters

Water that is a mixture of the two basin end members occurs in Fram Strait (Fig. 2) at 78°50′N. How far to the north and south can these mixed waters be found and where does the mixing take place? To address this, we present the average of five meridional CTD sections along 0°E (Fig. 7). Note that a few miles further west than 0°E, the water can pass horizontally around the Høvgaard fracture zone at 2500 m depth into the Greenland Sea (Fig. 1). The sections extend over 5-years (1997–1999, 2001–2002). The temperature increase over this period (Fig. 3) is evident when comparing the individual sections. However, all sections share the qualitative spatial patterns of temperature, salinity, and density discussed below.
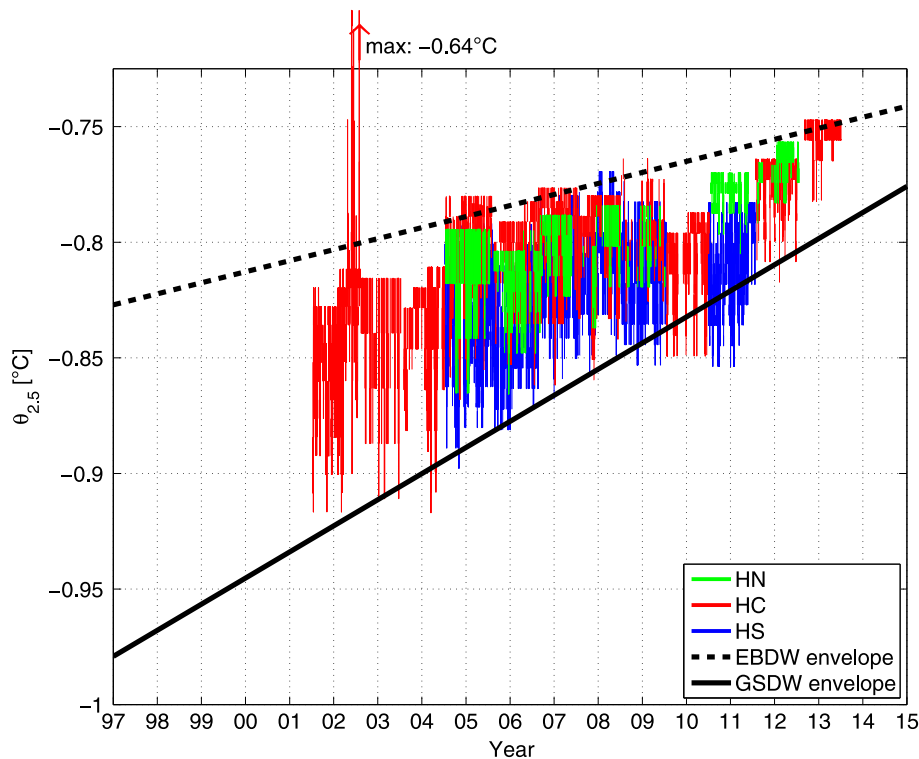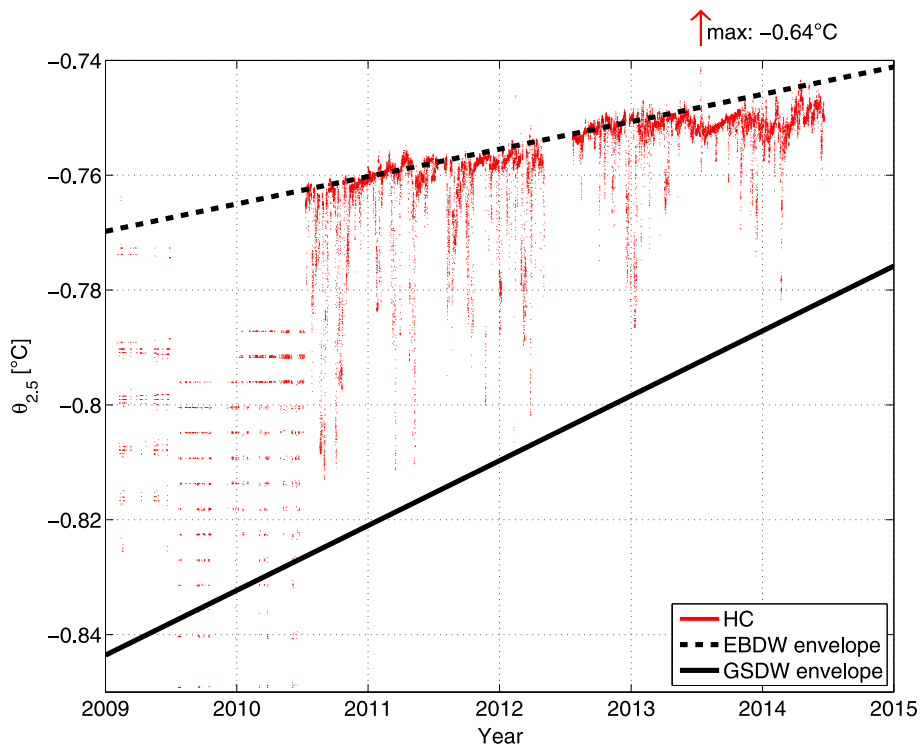

Fig. 5. Potential temperature timeseries of the RCM current meters as in Fig. 3, but for the three Hausgarten moorings to the north and south of the main zonal section. The envelopes for the GSDW and the EBDW end members are shown in black identical to Fig. 3. In 2002, the Storfjorden plume reaches two short peaks of −0.67 °C and −0.64 °C.

Fig. 6. Potential temperature timeseries as in Fig. 5, but at mooring HC showing each individual measurement as a dot. Temperature was measured by current meters in the deployment years 2008–2009 and 2009–2010. The striped horizontal lines separated by $\Delta\theta_{2.5} \approx 0.05\ ^\circ C$ correspond to the temperature resolution of the current meters. Temperature was measured by microcats with a much higher resolution in the deployment years 2010–2011, 2011–2012, 2012–2013, and 2013–2014. In 2013, the Storfjorden plume reaches a peak of $-0.64\ ^\circ C$.

Colder fresher water is to the south of the sill and warmer saltier water to the north (Fig. 7). At ≈ 2500 m and 78°N, the temperature and salinity in the sections (Fig. 7) is close to the Greenland Sea basin TS around 1997–2002 (compare Fig. 2). Likewise, at ≈ 2500 m and 79°40′N, the temperature and salinity in the sections corresponds to the Eurasian Basin basin TS at those times. The density lines, however, are relatively flat. This implies that, at sill depth, there is no north-south in situ density gradient across Fram Strait. This presentation supports and reaffirms the large scale temperature and salinity distribution across the Nordic Seas and the Arctic Ocean as shown by Aagaard et al. (1985). However, it also highlights the small horizontal scale over which the transition between the two water masses (GSDW to EBDW) takes place: about 20–30 nautical miles (minutes) near the sill of Fram Strait (between about 78°40′N and 79°00′–79°10′N).

Do the mooring records support the inference of this high localization of the meridional property gradients? In order to investigate the distribution of temperatures with respect to the end members, which are both warming at their own rates, we normalize the observed potential temperature $T_{obs}(t)$ at time t by the mean $T_{mean}(t)$ of the two end members and the difference $T_{diff}(t)$ between the two end members to define a quantity called "normalized temperature" $T_{norm}(t)$:

$$T_{norm}(t) = \frac{T_{obs}(t) - T_{mean}(t)}{\frac{1}{2}T_{diff}(t)} = \frac{T_{obs}(t) - \frac{1}{2}[T_{EBDW}(t) + T_{GSDW}(t)]}{\frac{1}{2}[T_{EBDW}(t) - T_{GSDW}(t)]} \quad (1)$$

Here $T_{GSDW}(t)$ and $T_{EBDW}(t)$ are the potential temperatures of the end members at time t. Using this definition, a normalized temperature of $+1$ corresponds to pure EBDW (identical to being on the EBDW envelope in Fig. 4), -1 corresponds to pure GSDW, and 0 refers to water coinciding with the mean of the two envelopes as indicated in Fig. 4.

A cumulative histogram of this normalized temperature is

shown in Fig. 8. For comparison, the error function is also shown which is the cumulative distribution function of the normal distribution. If the curves of the observed temperatures would fall onto the error function, then the temperatures were purely randomly distributed around the mean of the envelopes with ± 1 standard deviation of the observations corresponding to the EBDW and GSDW envelopes.

In the western Fram Strait (F9–F10), the distributions are very close to the error function indicating that neither end member dominates, but the water instead is a random mixture of the two end members. It also shows that the pure end members themselves occur fairly seldom. This contrasts with the visual conclusion that might be gained from Fig. 3 which as a result of the way the data is plotted overemphasizes the extreme values. We also note that this is not a result of how the end members were defined (2nd and 98th percentiles of running temperature distributions), as this definition would equally work for a bimodal distribution in which case both end members would be associated with distinct peaks in the running temperature distributions. The distributions of the observed temperatures (Fig. 8) instead are unimodal with a peak near a normalized temperature of 0. In the central and eastern Fram Strait (F7/8, F15/16) excluding F6, the curves again are qualitatively similar to each other. However, only about 40% of the water is colder than the average of the envelopes and the average temperature is closer to EBDW than to GSDW (average of normalized temperature is 0.1).

From this we conclude that the water at the mooring locations (F7–10, F15/16), i.e. on the plateau in Fram Strait, is mostly a mixture between the two end members. The mixing itself occurs over a larger region than just near the sill. The pristine end members show up more frequently at F9 and F10 compared to further east, i.e. the individual measurements near the normalized temperature of -1 (the GSDW end member) are more frequent. The water in the center of the strait (moorings F7–F16) is more
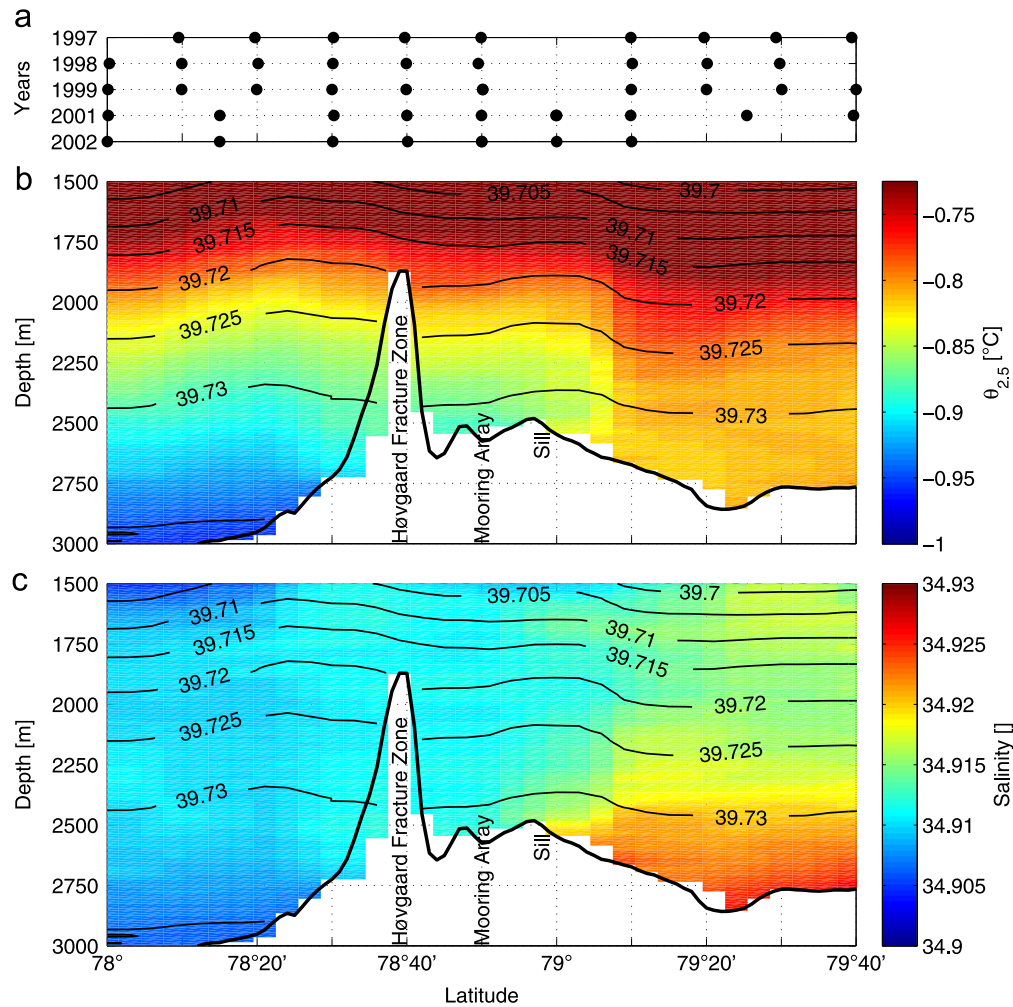
Fig. 7. Meridional sections of (b) potential temperature $\theta_{2.5}$ [°C] and (c) salinity [] along 0°E averaged over the years 1997, 1998, 1999, 2001, and 2002. The station locations in the respective years are marked in (a). Potential density $\sigma_{2.5}$ [kg/m³] is overlaid in contours on both panels.

mixed than further west. Only in the east (F6), warmer water than at the other moorings is measured as indicated by the fact that the curve of F6 is shifted to the right compared to the error function (Fig. 8; 20% of the observations lie above the normalized temperature of 1). Part of this is accounted for by the instruments at F6 during the 1999–2000 and 2007–2009 deployment periods (compare Fig. 3) which probably had calibration problems.

Compared to the Hausgarten records, the records along the main zonal section are much more similar to each other. However, only a small distance to the south at HS, the record is much more dominated by GSDW (65% colder than a normalized temperature of 0). To the north, on the other hand, HC and HN only registered water colder than a normalized temperature of 0 for 25% and 15% of the time, respectively. In fact, the additional microcat measurements with a much higher temperature resolution available from 2010 to 2014 at HC (Fig. 6) show that the temperature at HC is often almost identical to the EBDW end member.

This confirms the structure of the meridional gradient as seen in the CTD sections (Fig. 7). Water that is in-between the two end members is prominent only in the vicinity of the Fram Strait plateau.
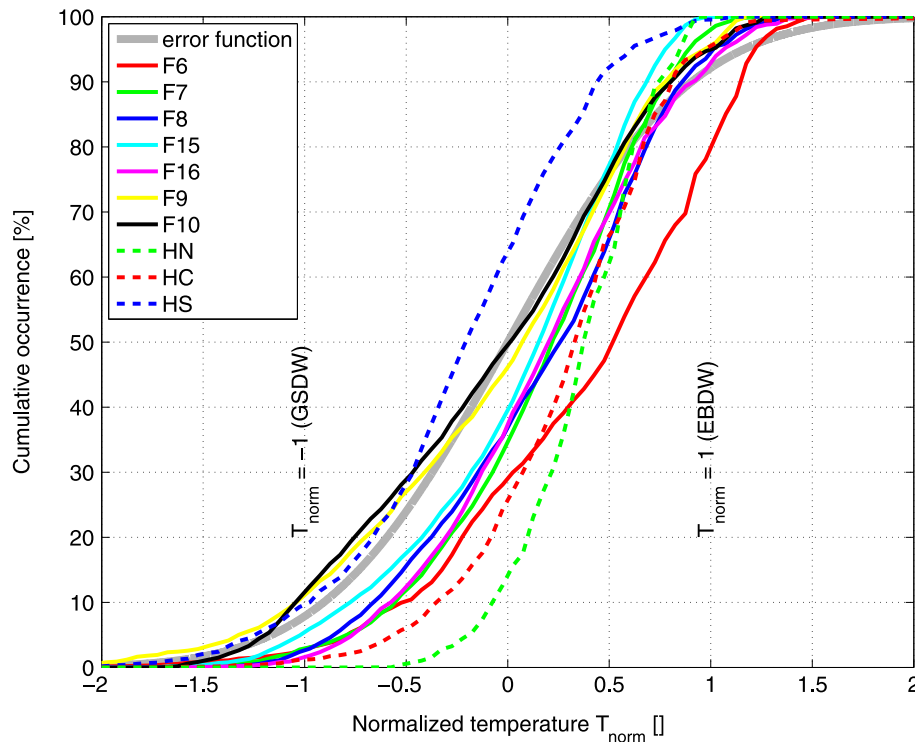
The distributions of the normalized temperature do not change significantly over time (not shown) and are always qualitatively similar to the error function as in Fig. 8. This means that at all times, there is mixed water with temperatures intermediate between the temperatures of the two end members (Fig. 3).

Additionally, both end members and the mixed water warm. From this we deduce that mixed water is continuously formed in and also exported from Fram Strait. If this was not the case, i.e. mixed water was just stagnant in Fram Strait, it would not change its temperature and would therefore over time have a temperature below the GSDW envelope. Hence, the previously formed mixed water needs to be exported from Fram Strait and new mixed water needs to be formed subsequently.

The $\theta_{2.5}$S curves of the individual CTD profiles of the meridional sections in 1997 and 1999 (Fig. 9) highlight that only one CTD profile at these sections falls between the end member profiles typical of the Greenland Sea to the south and the Eurasian Basin to the north. The "mixed water" profile in 1997 near the sill is smooth in the vertical and falls roughly between the two well defined basin profiles. Conversely, the profile in 1999 shows evidence of interleaving between the two basin profiles. Its $\theta_{2.5}$S properties switch back and forth between the two basin profiles over a relatively short vertical distance.

Interleaving between two water columns with different TS, but roughly the same density is indicative of a low energy environment (Rudels et al., 2015). If the mixing otherwise is strong, interleaving cannot take place (or it cannot be maintained for long). The profile in the vicinity of the sill from 1999 (Fig. 9b) is the only one showing a clear signature of interleaving while the other four central profiles (1997/1998, 2001/2002) of the five meridional sections are qualitatively similar to the 1997 profile (Fig. 9a) and

Fig. 8. Cumulative histograms of the normalized temperature (see Eq. (1)) of the near-bottom mooring records. Curves for the different moorings are shown in the same colors as in Figs. 3 and 5 and the time periods over which the distributions are shown are the same as plotted in those figures. The records from the main zonal section are solid and the Hausgarten records are dashed. Only the RCM current meter data is used here. For comparison, the error function is also shown in gray which would apply if the distributions were Gaussian with mean zero and standard deviation one. (For interpretation of the references to color in this figure legend, the reader is referred to the web version of this article.)

lack an interleaving signature. This corroborates the findings from the distributions of the normalized temperature (Fig. 8) that most of the water found near the sill is well mixed between the two end members while the two end members only infrequently show up at the sill. Hence we conclude that the mixing near the sill is relatively strong and effective in producing a new mixed water mass. It has been speculated (Swift and Koltermann, 1988) that this mixing in Fram Strait is the source for the Norwegian Sea Deep Water. This will be discussed further in Section 6.

5. Structure of the velocities achieving the exchange across Fram Strait

Direct measurements of turbulence in the deep Fram Strait are not available, so we discuss what the velocity records can tell us about the mixing and exchange. In Denmark Strait, the advective velocities associated with mesoscale variability (at a period of about 4 days; Macrander et al., 2007) can advect water parcels across the strait, i.e. from the basin to the north of the strait to the basin to the south of it. Since the excursion distance of these mesoscale motions is larger than the sill region (here the sill region is defined as the region with water depths close to the sill depth), the mixing between the water masses originating from the two basins occurs downstream of the strait region. In other oceanic straits (e.g. Price and O'Neil Baringer, 1994), mean flows advect water parcels across the sill region and the mixing also occurs downstream. We ask whether the situation in the deep Fram Strait is similar. What drives the exchange across the sill and where does the mixing occur?

The exchange across Fram Strait could be due to the mean flow or due to time-variable flows. If time-variable flows are important, it is of interest to determine which frequencies contribute to the

exchange and what drives the time-variable flows. Possible driving mechanisms for the time-variable flows include deep ocean density gradients and the associated pressure gradients as well as basin-scale externally forced motions such as Kelvin and topographic Rossby waves. Finally, also the surface flows might drive the deep velocities if the system is equivalent barotropic, i.e. if the current direction, but not necessarily the speed is mostly uniform throughout the water column. All of these mesoscale mechanisms will lead to horizontal shear and can therefore produce filaments which small scale processes can act upon to achieve the final mixing. Each of these possible driving mechanisms would have a particular signature in the velocity records as described now.

The mean near-bottom velocities in Fram Strait (Fig. 10) show a strong propensity for along-isobath flows. Northward flow prevails in the east, in the center generally westward flow is observed, and the flow in the west is southwards. This means that the mean-bottom flow is in a similar direction as the mean near-surface flow, however, with smaller amplitudes (compare e.g. Beszczynska-Möller et al., 2012). This suggests that the mean flow in Fram Strait has a strong equivalent barotropic component.

Hence, at the offshore foot of the West Spitsbergen Current in 2500 m depth, with the flow being along topography and northward around 2500 m (approximate sill depth), one would expect GSDW to be advected northwards along the continental slope and to then be detectable at mooring HC prominently. However, at HC, the water is almost purely EBDW with only short intermittent pulses of colder water containing some percentage of GSDW (Fig. 8). Since GSDW is mostly absent at HC (Fig. 8), we conclude that the mean flow is rather inconsequential to the exchange of deep waters across Fram Strait. The mean flow appears to be locally topographically steered, but does not achieve the cross-sill advection.

In order to investigate the temporal scales of motions affecting
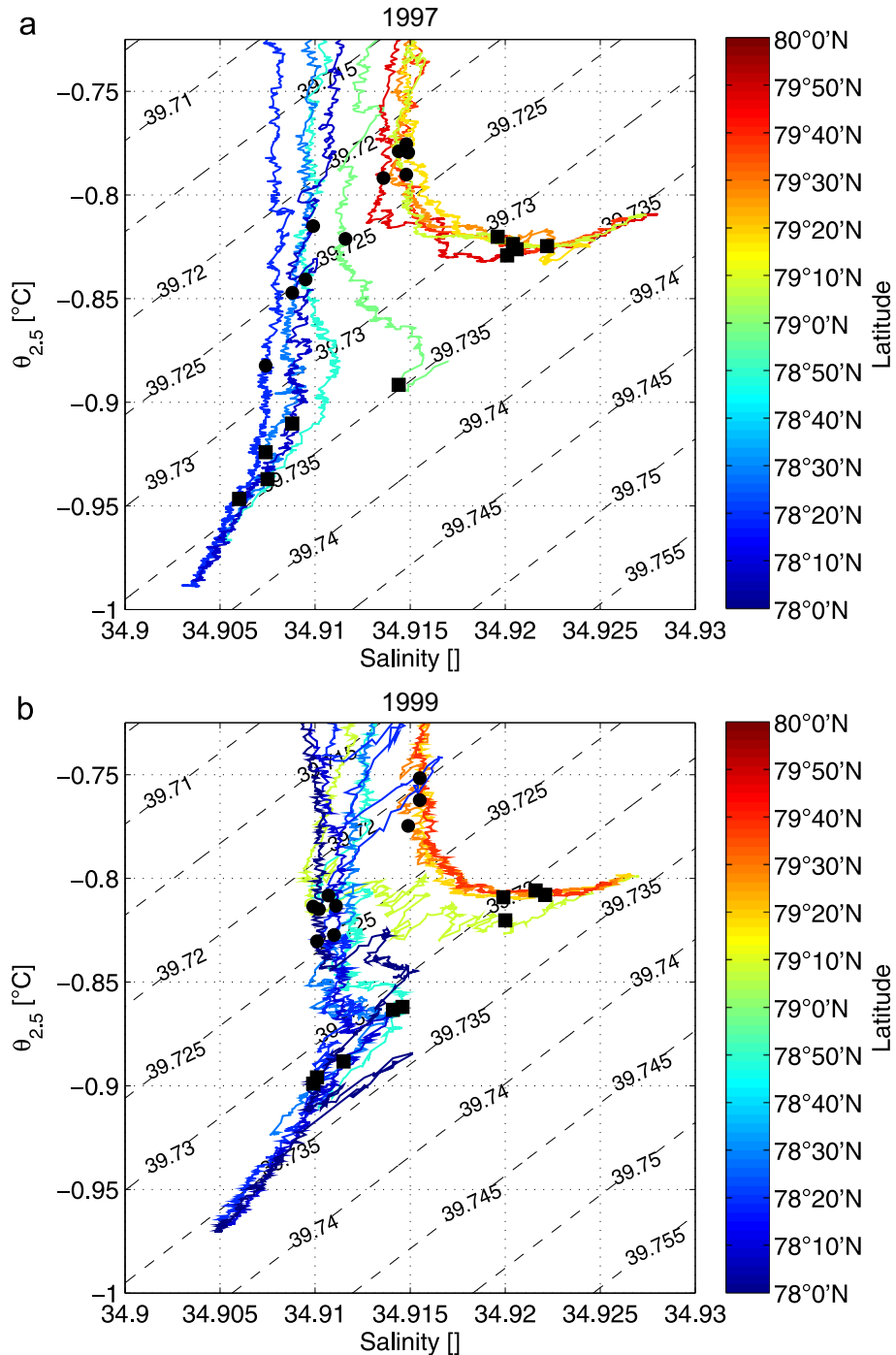
Fig. 9. CTD profiles in $\theta_{2.5}$S-space of the meridional section along 0°E in (a) 1997 and (b) 1999. The colors of the profiles refer to their latitude. The black dots and squares refer to the $\theta_{2.5}$S of the profiles at 2000 m and 2500 m, respectively. (For interpretation of the references to color in this figure legend, the reader is referred to the web version of this article.)

the deep water flow, we consider the integral time scales of the alongstream and cross-stream components of the bottom velocities. They are estimated using a simple auto-correlation of the velocity records. They vary between 5 days and 16 days. The period of a variable flow is approximately twice its integral time scale. This means that the associated time-variable motions have longer periods than the tidal/daily frequency band and shorter periods than the seasonal band. In fact, this long auto-correlation is due to northward or southward flow events lasting 3 days to 2 weeks which are discernible in the original velocity timeseries (not shown).

What is the meridional excursion distance associated with the variability in the several days band? The excursion distance of a periodic flow during half of its period is about 1/2*period*0.9*-standard deviation of the velocity (the factor of ≈ 0.9 comes from the integration over a sine wave). We consider the 3–30 days bandpass filtered bottom northward velocity timeseries (alongstream velocity timeseries show essentially the same numbers). The standard deviation in this frequency band ranges from 0.025 m/s at F6 to 0.04 m/s at F10 with a roughly monotonic increase towards the west. For example, for a period of 20 days and a standard deviation of 0.04 m/s, the excursion distance is
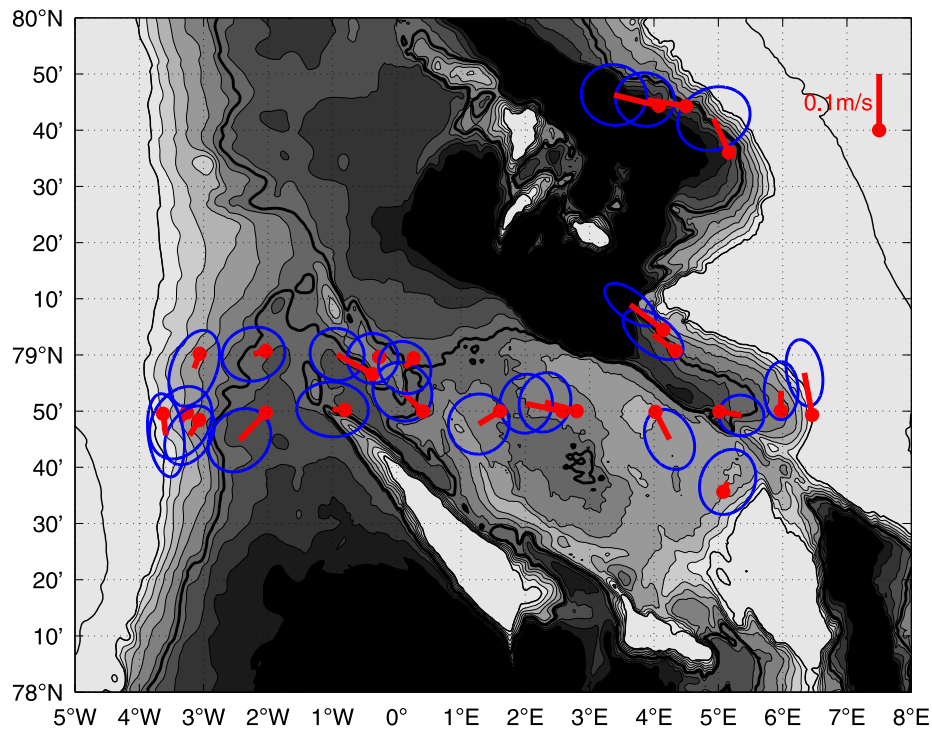
Fig. 10. Near-bottom (less than 100 m above the bottom) velocities as measured by the current meters on the moorings (compare Table 1 for the latitude/longitude/depth ranges) in the Fram Strait region. The mooring position is shown as a thick red dot and the record mean current vector is a thick red line pointing away from that location. The standard deviation ellipses around the mean are shown as blue lines. A scale bar of 0.1 m/s northward flow is shown in the top right corner. Individual moorings from different years that are less than 2 nautical miles apart are plotted at the same location in order to reduce the business of the figure while still maintaining a spatial view of the flow; for larger horizontal separations they are plotted separately. (For interpretation of the references to color in this figure legend, the reader is referred to the web version of this article.)

approximately 34 km or a bit less than 20 min of latitude. Likewise, for a period of 8 days and a standard deviation of 0.025 m/s, the distance is approximately 9 km or 5 min of latitude. The latitudinal extent of the sill is about 30 min (Fig. 1). Similarly, the latitudinal extent over which mixed water is found in the meridional CTD sections is approximately 20 min (Fig. 7). It can hence be concluded that events with periods and amplitudes at the high end of the observed spectrum can transport water across the plateau region of Fram Strait. The other more common motions only move the water for significant distances back and forth on the plateau. The periodic motions could also cause mixing through the interaction of the flow with the rough bottom. Another source of mixing may be the breaking of the M_2 internal tide for which the critical latitude (latitude at which the inertial frequency equals the M_2 frequency) of 74.5°N is only a few hundred kilometers to the south. Tides have also been identified as a source of energy for mixing on the Yermak Plateau north of the Fram Strait sill (Fer et al., 2014).

What is the source of the deep ocean flows with periods of 1–3 weeks? They could be due to local deep ocean dynamics or they could be remotely forced either by upper ocean mesoscale flows or by basin scale topographic Rossby waves excited by synoptic atmospheric forcing. If the deep ocean density gradient would drive the deep velocities, the motions should be coherent with variations in the temperature field and temperature variations should lead velocity variations. Conversely, deep velocity variations leading deep temperature variations would be indicative of the density field being advected by the velocities driven through another process. If, on the other hand, the deep flows are forced by the upper ocean, the upper ocean velocities and the deep ocean velocities should be coherent in the vertical. Coherence between the deep ocean velocities at different moorings separated by more than a few Rossby radii would be suggestive of a forcing by basin

scale wave motions. A purely deep ocean dynamical generation mechanism would show neither of these coherent signals.

We investigate the cross-correlation of the near-bottom velocities and the normalized temperature. An anti-correlation at a lag of ≈ -1 day (Fig. 11) is statistically significant at four of the moorings located in the western and central Fram Strait (F9/10, F15). The cross-correlation is highest for F9 and F10 in the western Fram Strait and in all cases positive velocity variations lead negative temperature variations, i.e. a northward flow is followed a day later by a temperature decrease, and vice versa. This is the opposite of what would be expected for a flow field driven by density gradients. Hence the flow field advects the density field consistent with the fact that the meridional density gradient is very weak (Fig. 7). Since the maximum cross-correlation may not be achieved for purely meridional flows, the velocity component that maximizes the absolute value of the cross-correlation was determined. It varies between 34° west of north and 56° east of north (Fig. 11) for the maximum anti-correlation near a lag of -1 day. That is, it is much closer to north than the mean velocities at the moorings (compare Fig. 10). This is a consequence of the combined effects of the prevailing north–south temperature gradient and the prevailing along-topography flows. However, while the correlations are significant, the values of -0.3 to -0.15 are small indicating the presence of a lot of additional processes, i.e. the exchange processes are not the sole dominating signal as they are in some other oceanic straits (e.g. Denmark Strait). For the ease of presentation, in the following, we only consider the meridional component of the velocity noting that the qualitative results below do not change when considering the component of maximum cross-correlation.

The coherence of the bottom northward velocity and the negative of the normalized temperature in the western Fram Strait at F10 (Fig. 12) is significant at periods between 3 days and 30 days
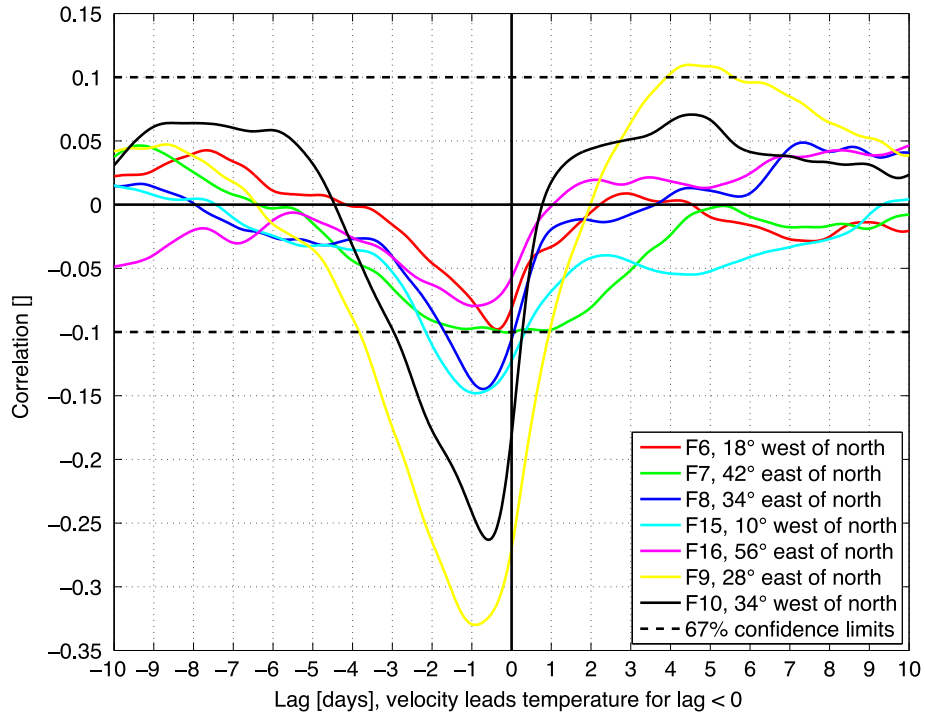
Fig. 11. Cross-correlation of bottom velocity components and the normalized bottom temperature records at each of the moorings. The plotted correlations are the average of the correlations of six months chunks of the unfiltered timeseries. The confidence limits have been estimated from a Monte Carlo simulation randomly varying the lags between the different timeseries. The velocities have been rotated by the angle indicated in the legend in order to maximize the observed anti-correlation.
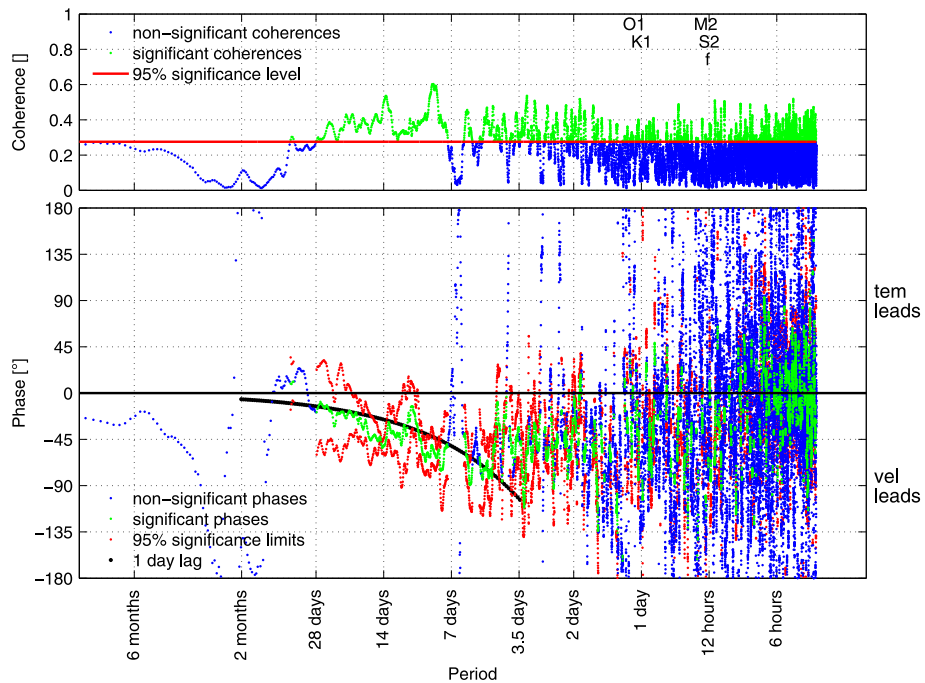
Fig. 12. Coherence of bottom northward velocity and the negative of the normalized bottom temperature at mooring F10 estimated using the Thomson multitaper method. The x-axis is logarithmic. Coherences (top panel) and their phases (bottom panel) that are significant at the 95% confidence level based upon a Monte-Carlo simulation are marked in green, non-significant ones in blue. The confidence limits around the phases are marked in red, that is, to 95% confidence, the phase is within the range indicated by the red curves. The phases corresponding to a 1 day lag are shown as a thick black line. The timeseries have been 365 days high-pass filtered before the coherence analysis. (For interpretation of the references to color in this figure legend, the reader is referred to the web version of this article.)

(with the exception of a small band between 5 days and 7 days that might be due to random statistics). The phase is around $-45°$ (closer to $0°$ for longer periods and approaching $-90°$ for shorter periods). Hence, the phase is always such that is corresponds to a 1 day lag (black line in Fig. 12). This means that, in this frequency band, a maximum of northward velocity is followed by a minimum in bottom temperature about 1 day later. This is consistent with the ≈ -1 day lag observed for the maximum anti-correlation between the velocities and the bottom temperatures (Fig. 11). The lag of -1 day and the $-45°$ phase offset shows that the velocities
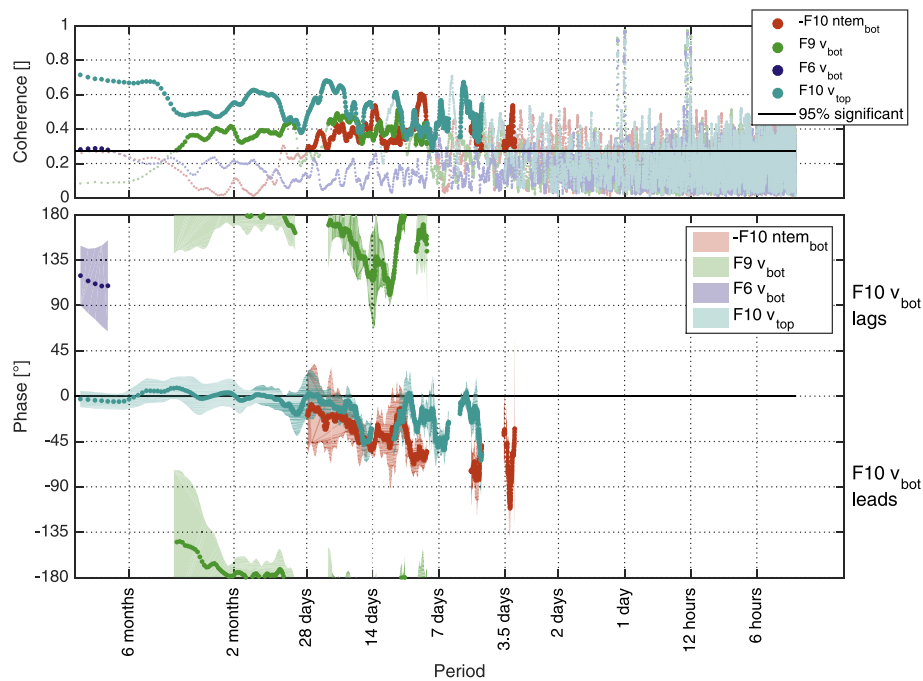
Fig. 13. Coherence of bottom northward velocity at F10 with four different timeseries: the negative of the normalized bottom temperature (red, this is identical to what is presented in Fig. 12), the bottom northward velocity at F9 (green), the bottom northward velocity at F6 (blue), and the near-surface (≈ 75 m depth) northward velocity at F10 (cyan). The coherences (top panel) are shown in thick saturated lines in bins where more than 90% of the estimates in a bin are above the 95% significance limit (thin black line). The bins are defined to encompass all frequencies between f_1 and f_2 such that $\log_{10}(f_2) - \log_{10}(f_1) = 0.05/\text{day}$. The phases (bottom panel) are only plotted for those significant conditions and the 95% confidence limits of the phase are indicated by the light shading around the best estimate of the phase. (For interpretation of the references to color in this figure legend, the reader is referred to the web version of this article.)

lead the temperature. The temperature variability in the 3–30 days frequency band can be explained through advection, as advection can cause these phase offsets. The coherences at the other moorings (not shown) are qualitatively similar, but, except for F9, not quite as significant in the 3–30 days frequency band. This is due to the lower velocities and stronger influence of the topography (Fig. 10) and is also evident in the lower cross-correlations (Fig. 11).

The horizontal coherence of the bottom northward velocities between different moorings depends on the distance between the moorings (Fig. 13). There is essentially no statistically significant coherence for large horizontal distances. F10 and F6 are ≈ 150 km apart which corresponds to many Rossby radii. Except for periods of more than half a year, they are not coherent. Since basin-scale waves that are forced remotely would be coherent across Fram Strait, we conclude that basin-scale waves do not contribute to the forcing of the bottom velocity variability. The bottom flows of neighboring moorings (Fig. 13), on the other hand, are coherent over a wide range of frequencies from periods of a week to several weeks. F10 and F9 are ≈ 25 km apart which is about 3 Rossby radii for a typical Rossby radius of 8 km in Fram Strait (Zhao et al., 2015). The phase difference is around 180°, that is when the velocity is northward at one of the moorings, it is southward at the other, and vice versa. This is typical of mesoscale motions in the sense that the flow is in opposite directions on either side of a mesoscale eddy and mesoscale eddies have typical diameters of ≈ 3 Rossby radii.

The bottom northward and the near-surface (≈ 75 m depth) northward velocities are statistically significantly coherent for all moorings at all periods longer than 3 days as well as at the tidal periods of the O_1, K_1, M_2, and S_2 tides (example for F10 in Fig. 13). The phase lags are 0° for the tidal periods (not visible in Fig. 13) and for periods longer than 30 days. However, in the band of 3–30 days, the phase varies between 0° and $-45°$ which would indicate that the bottom velocities lead the top velocities by an eighth of a

cycle. However, the confidence limits are not narrow enough around the signal to rule out that there is no phase lag between the two records. This shows that the velocities are highly correlated with each other in the vertical (equivalent barotropic). In other words, whatever happens at the periods relevant for the bottom temperature evolution is related to the near-surface flows.

From this, we rule out that the bottom velocities are driven by deep ocean temperature/density gradients or by basin-scale waves. Instead, surface mesoscale motions seem to drive the flow at the bottom which advects deep waters with contrasting TS properties across the sill region of Fram Strait.

6. Discussion

6.1. Summary

Temperature and velocity records in the deep Fram Strait near the sill level of 2545 m from 1997 to 2014 have been investigated in this study. The temperatures increase in accordance with the warming of Greeenland Sea Deep Water and Eurasian Basin Deep Water, water masses which were both observed immediately north and south of the sill region. The water near the sill is well-mixed, but the mixing is confined to this hot spot of mixing on the plateau region of Fram Strait. A coherence analysis suggests that the exchange across the sill is driven by mesoscale upper ocean flows.

6.2. Fate of the mixed water

This study raises at least three questions which are not resolved at this point in time. The warming rate of GSDW is faster than that of EBDW so that, at the current rates, the end members would reach the same temperature in 2020 (Section 3). This is also
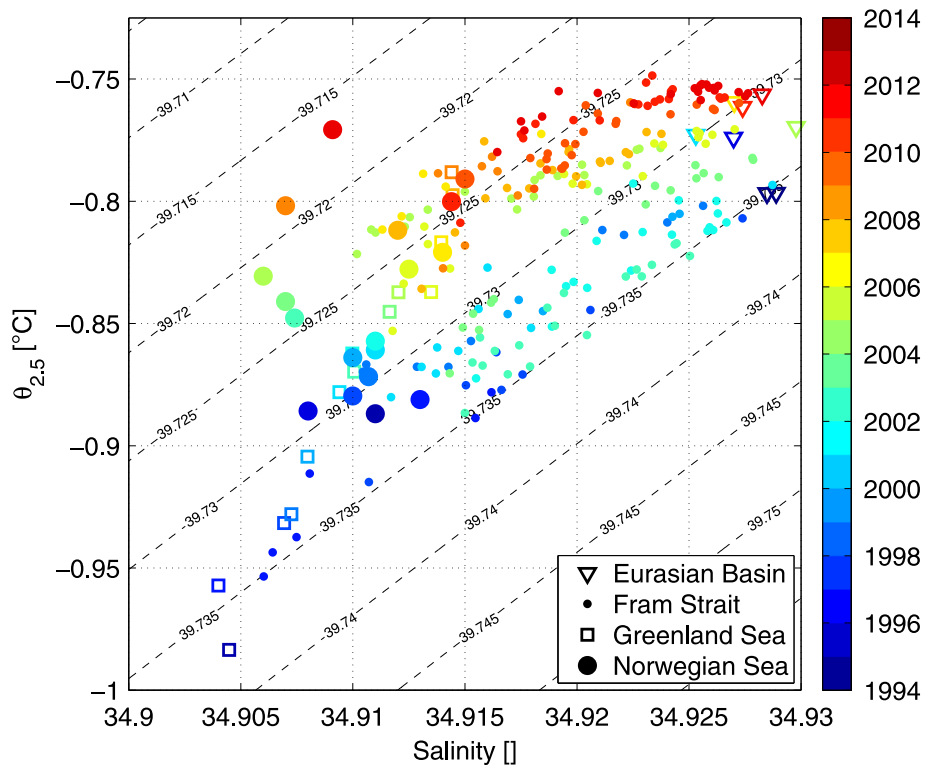
Fig. 14. Figure identical to Fig. 2, but also showing the means over the basin of the depth averaged (2500–2525 m) potential temperature and salinity of all CTD profiles in the Norwegian Sea (north of 66°N and east of 7°W) as big filled circles. Limiting the domain of the Norwegian Sea to between 70°N and 73°N and east of 0°E, i.e. approximately the Lofoten Basin does not change the figure qualitatively.

associated with a density decrease of GSDW compared to EBDW. It is therefore to be expected that the processes at Fram Strait will qualitatively change. It is also conceivable that the EBDW warming rate might increase as the Greenland Sea no longer cools the Eurasian Basin. However, the density difference between GSDW and EBDW was observed to have changed from ≈ -0.003 kg/m^3 in the mid 1990s to ≈ 0.007 kg/m^3 in the mid 2010s (Fig. 2). Even with this trend continuing, the density difference across the Fram Strait sill would remain almost two orders of magnitude smaller than the ≈ 0.4 kg/m^3 density difference across Denmark Strait driving the hydraulically controlled overflow there (Nikolopoulos et al., 2003). Hence density driven flows across Fram Strait will remain weak for the medium term future.

The actual rate of production of mixed water in Fram Strait is another question this study cannot answer. The absence of mean currents advecting the mixed water masses either to the north or south makes it impossible to estimate this production rate without a specific measuring campaign targeted to this question. Since the mixing region is rather localized on the plateau of Fram Strait, it would be conceivable that the rates are rather small.

The other obvious question stemming from this study is the fate of the mixed water present in the deep Fram Strait. It is not prominently present in the basins to the north or south (Figs. 2 and 8). Swift and Koltermann (1988) argued in the 1980s that the water mixed in Fram Strait is the origin of the deep waters in the Norwegian Sea. They proposed a cyclonic transport along the boundary of the Greenland Sea into the Norwegian Sea. However, this does not seem to have been the case after the 1990s. The mean temperature–salinity in the Norwegian Sea between 2500 m and 2525 m (Fig. 14) falls in between the GSDW and the EBDW end members in the 1990s, but is located closer to the GSDW than the mixed water in Fram Strait. This suggests that NSDW in the 1990s might have been formed from the mixed water in Fram Strait with more GSDW added during its passage through

the Greenland Sea. This would be consistent with the hypothesis of Swift and Koltermann (1988). However, since the mid 2000s, the Norwegian Sea temperature–salinity either agrees with the GSDW development (located on the same warming line of GSDW), or it is outside of the TS range defined by the end members and is instead shifted towards warmer and fresher conditions than GSDW and EBDW. Hence, the water in the Norwegian Sea in the 2000s and 2010s cannot have originated in Fram Strait, but may still be influenced by GSDW sometimes. This is consistent with the observed reversals of the flow direction in the Jan Mayen Channel connecting the Greenland and Norwegian Seas. The flow through the channel was observed to be towards the Norwegian Sea before 1992 and towards the Greenland Sea afterwards, although the amplitude was much reduced in the later period (Østerhus and Gammelsrød, 1999). The Fram Strait mixing product could also not be identified in other depth levels above 2500 m or below 2525 m. Therefore, we propose that the mixed water mass formed in Fram Strait might not make it around the cyclonic boundary current loop envisioned by Swift and Koltermann (1988) and instead gets mixed into the interior Greenland Sea where it could be acting as a heat source for the warming GSDW. The fact that it is not observed in the central Greenland Sea (Fig. 14) could be due to the fact that it is exported from Fram Strait along the East Greenland slope further to the west than the meridional section considered here (Fig. 7), but that it is also diluted with GSDW before reaching the central Greenland Sea. Especially if the actual production rates of the mixed water were very small, this appears to be a likely scenario.

References

Aagaard, K., Fahrbach, E., Meincke, J., Swift, J., 1991. Saline outflow from the Arctic Ocean: its contribution to the deep waters of the Greenland, Norwegian, and Iceland Seas. J. Geophys. Res.: Oceans (1978–2012) 96 (C11), 20433–20441.

Aagaard, K., Swift, J.H., Carmack, E.C., 1985. Thermohaline circulation in the Arctic Mediterranean Seas. J. Geophys. Res.: Oceans 90 (C3), 4833–4846.

Akimova, A., Schauer, U., Danilov, S., Núñez-Riboni, I., 2011. The role of the deep mixing in the Storfjorden shelf water plume. Deep Sea Res. Part I: Oceanogr. Res. Pap. 58 (4), 403–414.

Alford, M.H., Girton, J.B., Voet, G., Carter, G.S., Mickett, J.B., Klymak, J.M., 2013. Turbulent mixing and hydraulic control of abyssal water in the Samoan Passage. Geophys. Res. Lett. 40 (17), 4668–4674.

Bauerfeind, E., Nöthig, E.-M., Beszczynska, A., Fahl, K., Kaleschke, L., Kreker, K., Klages, M., Soltwedel, T., Lorenzen, C., Wegner, J., 2009. Particle sedimentation patterns in the eastern Fram Strait during 2000–2005: results from the Arctic long-term observatory HAUSGARTEN. Deep Sea Res. Part I: Oceanogr. Res. Pap. 56 (9), 1471–1487.

Beszczynska-Möller, A., Fahrbach, E., Schauer, U., Hansen, E., 2012. Variability in Atlantic water temperature and transport at the entrance to the Arctic Ocean, 1997–2010. ICES J. Mar. Sci.: J. Conseil 69 (5), 852–863.

de Steur, L., Hansen, E., Gerdes, R., Karcher, M., Fahrbach, E., Holfort, J., 2009. Freshwater fluxes in the East Greenland Current: a decade of observations. Geophys. Res. Lett. 36 (23).

Fer, I., Müller, M., Peterson, A., 2014. Tidal forcing, energetics, and mixing near the Yermak Plateau. Ocean Sci. Discus. 11 (5), 2245–2287.

Jakobsson, M., Mayer, L., Coakley, B., Dowdeswell, J.A., Forbes, S., Fridman, B., Hodnesdal, H., Noormets, R., Pedersen, R., Rebesco, M., et al., 2012. The international bathymetric chart of the Arctic Ocean (IBCAO) version 3.0. Geophys.

Res. Lett. 39 (12).

Johannessen, J., Johannessen, O., Svendsen, E., Shuchman, R., Manley, T., Campbell, W., Josberger, E., Sandven, S., Gascard, J., Olaussen, T., et al., 1987. Mesoscale Eddies in the Fram Strait Marginal Ice Zone during the 1983 and 1984 Marginal Ice Zone Experiments. J. Geophys. Res. 92 (C7), 6754–6772.

Langehaug, H.R., Falck, E., 2012. Changes in the properties and distribution of the intermediate and deep waters in the Fram Strait. Prog. Oceanogr. 96 (1), 57–76.

Macrander, A., Käse, R., Send, U., Valdimarsson, H., Jónsson, S., 2007. Spatial and temporal structure of the Denmark Strait overflow revealed by acoustic observations. Ocean Dyn. 57 (2), 75–89.

Manley, T., Hunkins, K., Villanueva, J., van Leer, J., Gascard, J., Jeannin, P., 1987. Mesoscale oceanographic processes beneath the ice of Fram Strait. Science 236 (4800), 432–434.

Marsh, R., Josey, S.A., de Cuevas, B.A., Redbourn, L.J., Quartly, G.D., 2008. Mechanisms for recent warming of the North Atlantic: insights gained with an eddy-permitting model. J. Geophys. Res.: Oceans 113 (C4).

Meincke, J., Jonsson, S., Swift, J.H., 1992. Variability of convective conditions in the Greenland Sea. In: ICES Marine Science Symposium, vol. 195, pp. 32–39.

Nikolopoulos, A., Borenäs, K., Hietala, R., Lundberg, P., 2003. Hydraulic estimates of Denmark Strait overflow. J. Geophys. Res. 108, 3095.

Østerhus, S., Gammelsrød, T., 1999. The abyss of the Nordic Seas is warming. J. Clim. 12 (11), 3297–3304.

Price, J., O'Neil Baringer, M., 1994. Outflows and deep water production by marginal seas. Prog. Oceanogr. 33 (3), 161–200.

Rhein, M., 1991. Ventilation rates of the Greenland and Norwegian Seas derived from distributions of the chlorofluoromethanes F11 and F12. Deep Sea Res. Part A: Oceanogr. Res. Pap. 38 (4), 485–503.

Rudels, B., Korhonen, M., Schauer, U., Pisarev, S., Rabe, B., Wisotzki, A., 2015. Circulation and transformation of Atlantic water in the Eurasian Basin and the contribution of the Fram Strait inflow branch to the Arctic Ocean heat budget. Prog. Oceanogr. 132, 128–152.

Schlosser, P., Bönisch, G., Rhein, M., Bayer, R., 1991. Reduction of deepwater formation in the Greenland Sea during the 1980s: evidence from tracer data. Science 251 (4997), 1054–1056.

Somavilla, R., Schauer, U., Budéus, G., 2013. Increasing amount of Arctic Ocean deep waters in the Greenland Sea. Geophys. Res. Lett.

Swift, J.H., Koltermann, K.P., 1988. The origin of Norwegian Sea deep water. J. Geophys. Res.: Oceans 93 (C4), 3563–3569.

Teigen, S., Nilsen, F., Gjevik, B., 2010. Barotropic instability in the West Spitsbergen Current. J. Geophys. Res. 115 (C7), C07016.

von Appen, W.-J., Schauer, U., Somavilla Cabrillo, R., Bauerfeind, E., Beszczynska-Möller, A., 2015. Physical oceanography and current meter data from mooring and CTD measurements at Fram Strait. Pangea . http://dx.doi.org/10.1594/PANGAEA.845938.

Zhao, M., Timmermans, M.-L., Cole, S., Krishfield, R., Proshutinsky, A., Toole, J., 2015. Characterizing the eddy field in the Arctic Ocean halocline. J. Geophys. Res.: Oceans.